The EMBO Journal Vol.18 No.1 pp.96–108, 1999

Quasi-synaptic calcium signal transmission between endoplasmic reticulum and mitochondria

György Csordás, Andrew P.Thomas and György Hajnóczky[1]

Department of Pathology, Anatomy and Cell Biology, Thomas Jefferson University, Philadelphia, PA 19107, USA

[1]Corresponding author
e-mail: hajnocz1@jeflin.tju.edu

Transmission of cytosolic $[Ca^{2+}]$ ($[Ca^{2+}]_c$) oscillations into the mitochondrial matrix is thought to be supported by local calcium control between IP_3 receptor Ca^{2+} channels (IP3R) and mitochondria, but study of the coupling mechanisms has been difficult. We established a permeabilized cell model in which the Ca^{2+} coupling between endoplasmic reticulum (ER) and mitochondria is retained, and mitochondrial $[Ca^{2+}]$ ($[Ca^{2+}]_m$) can be monitored by fluorescence imaging. We demonstrate that maximal activation of mitochondrial Ca^{2+} uptake is evoked by IP_3-induced perimitochondrial $[Ca^{2+}]$ elevations, which appear to reach values >20-fold higher than the global increases of $[Ca^{2+}]_c$. Incremental doses of IP_3 elicited $[Ca^{2+}]_m$ elevations that followed the quantal pattern of Ca^{2+} mobilization, even at the level of individual mitochondria. In contrast, gradual increases of IP_3 evoked relatively small $[Ca^{2+}]_m$ responses despite eliciting similar $[Ca^{2+}]_c$ increases. We conclude that each mitochondrial Ca^{2+} uptake site faces multiple IP3R, a concurrent activation of which is required for optimal activation of mitochondrial Ca^{2+} uptake. This architecture explains why calcium oscillations evoked by synchronized periodic activation of IP3R are particularly effective in establishing dynamic control over mitochondrial metabolism. Furthermore, our data reveal fundamental functional similarities between ER–mitochondrial Ca^{2+} coupling and synaptic transmission.

Keywords: calcium signal/endoplasmic reticulum/inositol trisphosphate/mitochondria/quantal calcium release

Introduction

Signal transmission between cells of multicellular organisms is often facilitated by privileged communications (e.g. synaptic transmission, paracrine control), which enhance the fidelity of signal recognition by target cells and decrease undesired effects on other cells. The same arrangements are emerging for intracellular signaling, particularly in the case of multifunctional second messengers such as Ca^{2+} or cAMP (reviewed in Berridge 1997; Houslay and Milligan, 1997; Pawson and Scott, 1997). Cytosolic $[Ca^{2+}]$ ($[Ca^{2+}]_c$) and cAMP increases mediate the effects of many extracellular stimuli on a diverse range of cell functions, including motility, secretion, metabolism, gene expression and proliferation. Targeting of the effects of cAMP can be established by localization of cAMP-dependent protein kinase to specific subcellular sites through the interaction of regulatory subunits with A-kinase anchoring proteins (reviewed in Lester and Scott, 1997). Compelling evidence has been presented recently that local spatial and temporal patterns of calcium signals are important in encoding the specificity of cellular responses (Tse *et al*., 1993; Hanson *et al*., 1994; Hajnóczky *et al*., 1995; Dolmetsch *et al*., 1997; De Koninck and Schulman, 1998; reviewed in Putney, 1998). In many cases, strategic localization of Ca^{2+} entry/release sites at the subcellular level may account for selective activation of specific processes.

Some calcium signals rely on stimulation of plasma membrane Ca^{2+} entry channels. In these cases, much larger increases of $[Ca^{2+}]$ can occur in the vicinity of the plasma membrane than the global increases of $[Ca^{2+}]_c$, and some Ca^{2+}-activated responses (e.g. secretion) may depend on the generation of such large localized calcium increases (Silver *et al*., 1990; Llinás *et al*., 1992; Marsault *et al*., 1997; contrary finding in Kim *et al*., 1997). Other forms of calcium signal rely on mobilization of Ca^{2+} from intracellular stores to fuel the $[Ca^{2+}]_c$ increases. Many hormones, neurotransmitters and growth factors stimulate IP_3 formation, which in turn activates Ca^{2+} release channels located predominantly in the ER. Calcium signals driven by IP_3 receptors were described first as global increases of $[Ca^{2+}]_c$, which were often manifested in the form of frequency-modulated Ca^{2+} oscillations propagating throughout the cell as calcium waves (reviewed in Cobbold and Cuthbertson, 1990; Berridge, 1993; Petersen *et al*., 1994; Clapham, 1995; Thomas *et al*., 1996). Such global $[Ca^{2+}]_c$ signals have been suggested to result from spatially and temporally coordinated recruitment of subcellular release units (Parker *et al*., 1996; Bootman *et al*., 1997). It is important to note that the cytoplasm is a relatively poor passive conductor for Ca^{2+} increases due to the large amount of Ca^{2+} buffering proteins, and conduction of IP_3-induced Ca^{2+} signals is an active, self-propagating process. Recently, elementary events of IP3R-driven $[Ca^{2+}]_c$ signals have been resolved as Ca^{2+} 'sparks', 'puffs' and 'blips'. These are believed to represent Ca^{2+} responses associated with activation of one or a few IP3Rs (Yao *et al*., 1995; Bootman and Berridge, 1996; Parker and Yao, 1996; Reber and Schindelholz, 1996; Horne and Meyer, 1997). During the brief periods of channel opening at the sites of the elementary Ca^{2+} release events, the local concentration rises to high levels before it dissipates into the surrounding cytoplasm. Within the microdomain of the elementary event, the high levels of Ca^{2+} may yield rapid and spatially limited changes in the activity of Ca^{2+}-regulated processes, which are less sensitive to Ca^{2+} than the processes controlled by the global Ca^{2+} signals.

Calcium is a well-known activator of mitochondrial dehydrogenases (for review see McCormack *et al*., 1990) and so Ca^{2+} could be an ideal signal to synchronize cell function and mitochondrial metabolism during stimulation by Ca^{2+}-mobilizing stimuli. Mitochondrial matrix $[Ca^{2+}]$ ($[Ca^{2+}]_m$) is regulated by specific Ca^{2+} transport pathways. The uptake of Ca^{2+} is driven by the membrane potential and is mediated by an electrogenic uniport. The egress of mitochondrial Ca^{2+} occurs via distinct Na^+-independent and -dependent carriers (reviewed in Gunter *et al*., 1994; Pozzan *et al*., 1994). Considering that the rise of global $[Ca^{2+}]_c$ to between 500 nM and 1 μM during IP_3-activated $[Ca^{2+}]_c$ signals is probably not sufficient to activate the low-affinity mitochondrial Ca^{2+} uptake mechanisms, mitochondria were believed to be relatively insensitive to physiological $[Ca^{2+}]_c$ increases. A major breakthrough was achieved using aequorin targeted to the mitochondrial matrix. Rizzuto, Pozzan and co-workers demonstrated that mitochondria undergo a large increase of $[Ca^{2+}]_m$ in response to stimulation with IP_3-linked stimuli in a wide variety of cells (Rizzuto *et al*., 1992, 1993, 1994). Furthermore, using fluorescent Ca^{2+}-tracers compartmentalized into the mitochondria, we achieved resolution of $[Ca^{2+}]_m$ at the single-cell level and demonstrated that the pulsatile release of Ca^{2+} underlying $[Ca^{2+}]_c$ oscillations driven by the IP3R is delivered efficiently into the mitochondrial matrix, giving rise to coupled oscillations of $[Ca^{2+}]_m$ (Hajnóczky *et al*., 1995). Through this process, a large activation of Ca^{2+}-sensitive steps of mitochondrial metabolism is achieved by IP_3-induced increases of $[Ca^{2+}]_m$ (Pralong *et al*., 1994; Hajnóczky *et al*., 1995), demonstrating a physiological role for mitochondrial Ca^{2+} signaling. It is also becoming apparent that mitochondria modulate cytosolic Ca^{2+} signaling (Jouaville *et al*., 1995; Budd and Nicholls, 1996; Babcock *et al*., 1997; Hoth *et al*., 1997; Ichas *et al*., 1997; Simpson *et al*., 1997). Taken together, these observations show that the release of Ca^{2+} from the ER in response to IP_3 is closely coupled with mitochondrial Ca^{2+} uptake in the cells, suggesting a privileged transfer of Ca^{2+} between ER and mitochondria. It has been proposed that mitochondria are exposed to microdomains of high $[Ca^{2+}]$ due to a close spatial coupling between IP_3-induced Ca^{2+} release sites and mitochondrial Ca^{2+} uptake sites (Rizzuto *et al*., 1993, 1994, 1998).

The major aim of this study was to determine the functional organization of Ca^{2+} transfer between IP3R and mitochondria. We established an experimental model that allowed us to monitor $[Ca^{2+}]_m$ responses evoked by IP_3 down to the level of single mitochondria. Using this model, we show that synchronous activation of IP3R results in a localized $[Ca^{2+}]$ increase at the ER–mitochondrial junction, which is sufficient to evoke maximal activation of mitochondrial Ca^{2+} uptake sites. Calibration of mitochondrial Ca^{2+} uptake by varying the extramitochondrial $[Ca^{2+}]$ showed that IP_3-induced Ca^{2+} elevation in the vicinity of the mitochondria can reach values >20-fold higher than the global increases of $[Ca^{2+}]_c$. We show that the quantal pattern of Ca^{2+} release evoked by submaximal IP_3 is associated with quantal elevations of $[Ca^{2+}]_m$, though low doses or gradual increases of IP_3 evoked relatively small $[Ca^{2+}]_m$ responses. We propose that Ca^{2+} release through multiple IP3Rs is integrated at each mitochondrial Ca^{2+} uptake site, so that optimal signal transmission is achieved during synchronous activation of multiple IP3Rs. Thus, the IP3R-mediated elementary Ca^{2+} release signals which represent the building blocks of cytosolic Ca^{2+} signaling may stimulate mitochondrial Ca^{2+} uptake on an individual basis, but recruitment of multiple elementary events leads to disproportionally larger mitochondrial $[Ca^{2+}]$ responses.

Results and discussion

Fluorescence imaging of $[Ca^{2+}]_m$ responses evoked by IP_3

In order to dissect the mechanisms underlying local Ca^{2+} regulation between IP3R and mitochondria, our first aim was to establish a permeabilized cell model in which mitochondrial $[Ca^{2+}]$ could be monitored fluorometrically and where the Ca^{2+} coupling between ER and mitochondria was preserved. We recognized that loading of mast cells (RBL-2H3 cells) with the acetoxymethyl ester form of fura2FF or rhod2 yielded compartmentalization of these dyes into mitochondria. Figure 1A shows fluorescence images of the distribution of the compartmentalized fura2FF in permeabilized mast cells. The spatial pattern of the mitochondria was visualized using fluorescence imaging of the vital mitochondrial dye MitoTracker Red in the same cells. Typically, oval-shaped mitochondrial cross-sections were detected (Figure 1A), although elongated mitochondria were also observed, particularly at the base of the cells. Using green fluorescent protein targeted to the mitochondria (mitoGFP), the same pattern of mitochondria was evident (Figure 2). It is also shown that the permeabilized preparation retained much of the mitochondrial morphology of the intact cells (Figure 2). Identical structures were found to be labeled with compartmentalized fura2FF and MitoTracker Red, suggesting that fura2FF was trapped in the mitochondria (Figure 1A, i and ii). Fura2FF fluorescence was relatively high using excitation of the Ca^{2+} free form (380 nm, green), whereas little fluorescence was obtained with excitation of the Ca^{2+}-bound form (340 nm, red), yielding a mainly green color when the two color images were overlaid (Figure 1Aii). Addition of IP_3 led to a rapid elevation of $[Ca^{2+}]$ measured by the fluorescence response of compartmentalized fura2FF (increase of the red component and decrease of the green component in Figure 1A, iii versus ii), whereas the Ca^{2+}-insensitive fluorescence signal of the MitoTracker Red was unchanged (Figure 1Av). The increase of $[Ca^{2+}]$ evoked by IP_3 was reversed after addition of a Ca^{2+} ionophore, ionomycin, demonstrating that the IP_3-induced elevation of $[Ca^{2+}]$ occurred in a non-acidic vesicular pool (Figure 1A, iv versus iii). Preincubation with mitochondrial uncouplers prevented the IP_3-induced changes of $[Ca^{2+}]_{fura2FF}$ (not shown). Fura2FF has been shown to become compartmentalized in the ER of hepatocytes (Hajnóczky and Thomas, 1997) and partly in the ER of astrocytes (Golovina and Blaustein, 1997), as judged by IP_3-induced decrease of $[Ca^{2+}]_{fura2FF}$, but addition of IP_3 was not found to exert such an effect in RBL-2H3 cells (Figures 1 and 3). Taken together, these data show the predominant mitochondrial localization of compartmentalized fura2FF and suggest that mitochondria respond to IP_3-induced Ca^{2+} release in permeabilized RBL-2H3 cells.

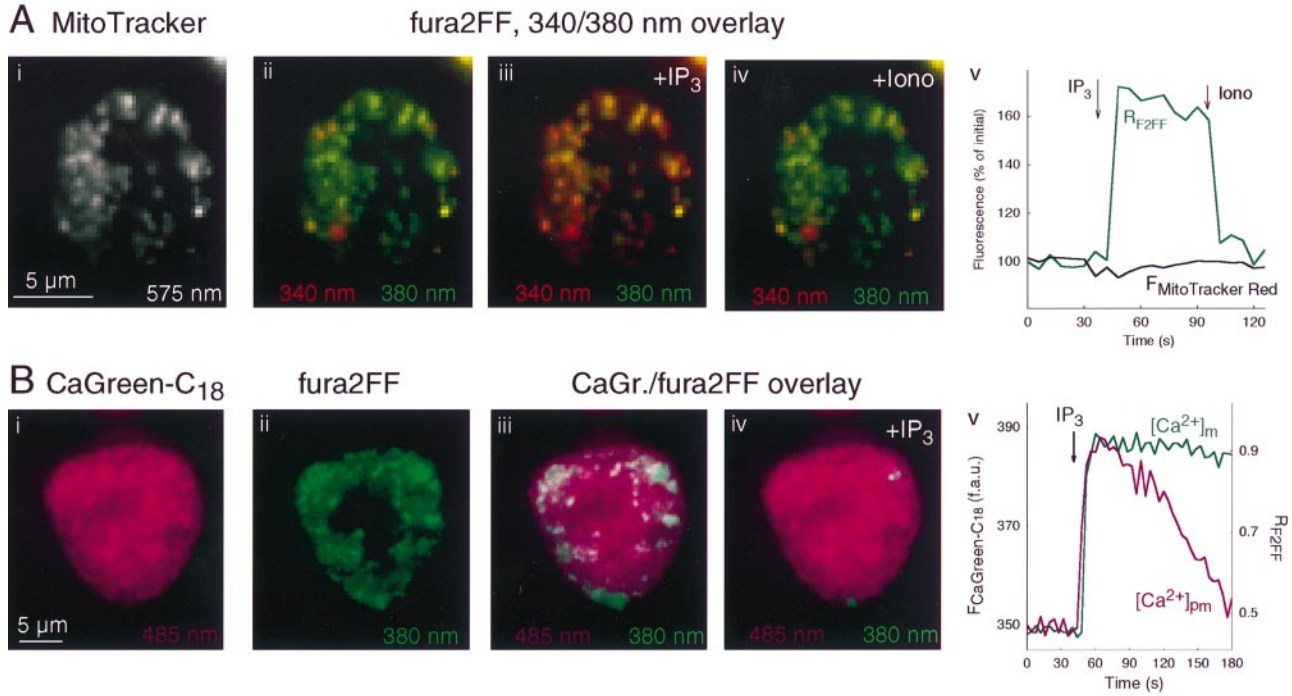

Fig. 1. Fluorescence imaging of $[Ca^{2+}]_m$ with compartmentalized fura2FF in single permeabilized RBL-2H3 cells. (**A**) The gray image (i) shows the distribution of mitochondria visualized by MitoTracker™ Red. The green (380 nm excitation)/red (340 nm excitation) overlay images (ii–iv) show the distribution of the compartmentalized fura2FF and the fluorescence changes upon addition of saturating IP_3 (ii–iii) and ionomycin (iii–iv), respectively. Time-courses of the fluorescence changes are plotted in panel v. (**B**) Fluorescence distribution of the lipophilic perimembrane Ca^{2+} indicator dye CaGreen-C_{18} (i and iii–iv, marked in purple) and of the compartmentalized fura2FF measured at 380nm excitation (ii–iv, marked in green) are shown. IP_3-induced flurescence changes are shown in the overlay images (iii–iv). In (v), time-courses of the fluorescence changes are shown.

Compartmentalized rhod2 was also found to occur in the organelles labeled with MitoTracker Green or mitoGFP (Figure 2D) and was found to measure mitochondrial uncoupler-sensitive $[Ca^{2+}]$ increases in response to IP_3 as well (Figure 2E). Nevertheless, fura2FF was used to monitor $[Ca^{2+}]_m$ in most experiments in the present study, because this dye can be used for ratiometric $[Ca^{2+}]$ measurements, and the lower affinity of fura2FF towards Ca^{2+} (K_d ~35 µM for fura2FF versus 1 µM for rhod2) is favorable in order to avoid saturation during large increases of $[Ca^{2+}]_m$. Indeed, the basal $[Ca^{2+}]_m$ was found to be in the discriminatory range of rhod2 (100–500 nM), but IP_3-induced increases of $[Ca^{2+}]_m$ led to saturation of rhod2 in many cells (not shown). Using fura2FF, IP_3-induced elevations of $[Ca^{2+}]_m$ did not cause saturation of the dye, and calibration of the fluorescence signals yielded values of 10–20 µM for the peak of $[Ca^{2+}]_m$, which are in good agreement with the $[Ca^{2+}]_m$ of ~15 µM reported in intact single cells stimulated with IP_3-linked agonists (Rutter *et al*., 1996).

In order to investigate further the role of Ca^{2+} release induced by IP_3 in the activation of mitochondrial Ca^{2+} uptake, fura2FF-loaded permeabilized RBL cells were exposed to Calcium Green-C18. The lipophilic alkyl chain anchors the Ca^{2+} indicator Calcium Green to the lipid membranes, allowing measurements of $[Ca^{2+}]$ immediately adjacent to cellular membranes (Tanimura and Turner, 1996). Calcium Green-C18 labeled cellular membranes throughout the cell, whereas the compartmentalized fura2FF showed a distribution that correlated with the mitochondria in the same cells (Figure 1B, i and ii). Addition of IP_3 caused an increase of perimembrane $[Ca^{2+}]$ ($[Ca^{2+}]_{pm}$) (increase of the purple component on Figure 1B, iv versus iii) and an increase of $[Ca^{2+}]_m$ (decrease of the green component on Figure 1B, iv versus iii). The increase of $[Ca^{2+}]_{pm}$ preceded the elevation of $[Ca^{2+}]_m$ and was transient (Figure 1B, v). The fall of $[Ca^{2+}]_{pm}$ could be due to Ca^{2+} uptake into other compartments or to dilution of released Ca^{2+} in the large bath volume. The latter explanation is supported by our finding that addition of uncoupler, or addition of an inhibitor of the sarco-endoplasmic reticulum Ca^{2+} pump, thapsigargin (Tg), to prevent re-uptake of Ca^{2+} released by IP_3, did not change the shape of $[Ca^{2+}]_{pm}$ transients markedly (not shown). Unexpectedly, the $[Ca^{2+}]_m$ signal induced by IP_3 showed prolonged elevation despite the decay of the $[Ca^{2+}]_{pm}$ rise (Figure 1B, v) suggesting a low activity of mitochondrial Ca^{2+} efflux. This could be explained by the loss of some regulatory factors during cell permeabilization, though cell-type specific differences in activation of mitochondrial Ca^{2+} efflux should also be considered, since $[Ca^{2+}]_m$ signals were more sustained in RBL-2H3 cells than that in permeabilized hepatic cells or cardiac myoblasts under comparable conditions (unpublished observation).

Transmission of $[Ca^{2+}]_c$ increases to the mitochondrial matrix

As a further approach to characterize the mechanism underlying propagation of IP_3-induced $[Ca^{2+}]$ increases into the mitochondria, $[Ca^{2+}]_c$ and $[Ca^{2+}]_m$ responses to exogeneous Ca^{2+} and IP_3 were compared in suspensions of fura2FF-loaded permeabilized RBL cells. Cytosolic $[Ca^{2+}]$ and $[Ca^{2+}]_m$ were measured simultaneously using

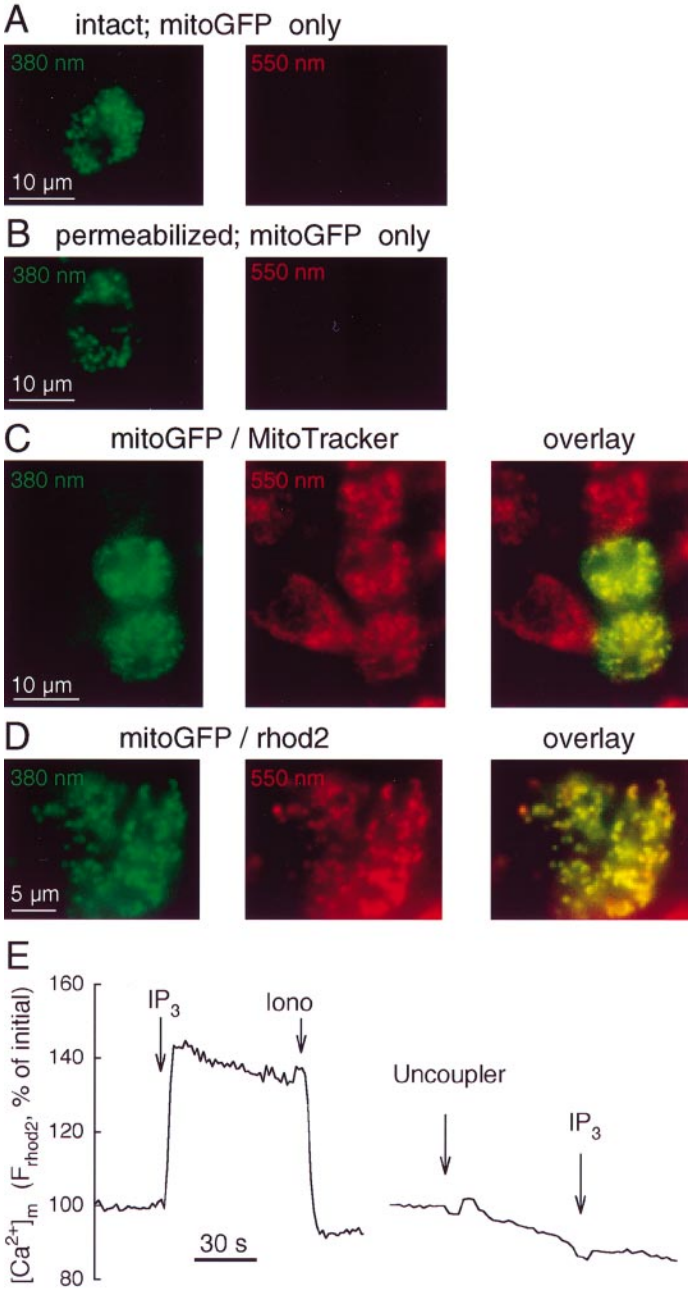

Fig. 2. Visualization of mitochondria by mitoGFP. Fluorescence images of (**A**) intact and (**B**–**D**) permeabilized mast cells transfected with mitoGFP. Cells were also loaded with MitoTracker Red (C) or rhod2/AM (D). The green images (380 nm excitation, left panels) show the distribution of mitoGFP, the red images (550 nm excitation, middle panels) show the distribution of MitoTracker Red (C) or compartmentalized rhod2 (D). These images are overlaid in the right panels to show the coincidence of the labeled organelles (overlay). (**E**) IP_3 (12.5 μM)-induced $[Ca^{2+}]_m$ responses recorded in the absence and presence of uncoupler (FCCP/Oligomycin, 5 μg/ml of each) using compartmentalized rhod2 in single permeabilized cells.

rhod2 added into the medium and compartmentalized fura2FF, respectively. In contrast to the imaging studies, intracellular Ca^{2+} stores were able to control global medium $[Ca^{2+}]$ (the cytosolic phase; $[Ca^{2+}]_c$) in the cell suspension studies, since the ratio of cell mass to bath volume was >20 times larger than that in the imaging experiments. Figure 3 shows that IP_3-induced Ca^{2+} release appeared as an increase of $[Ca^{2+}]_c$ and a subsequent increase of $[Ca^{2+}]_m$. Pretreatment with mitochondrial uncoupler abolished the IP_3-induced increase of $[Ca^{2+}]_m$, whereas the IP_3-induced $[Ca^{2+}]_c$ increase was slightly enhanced, presumably due to the absence of mitochondrial Ca^{2+} uptake (Figure 3). The IP_3-induced mitochondrial Ca^{2+} elevation was also inhibited by an inhibitor of the mitochondrial Ca^{2+} uniporter, ruthenium red (3 μM, Figure 3). Thus, IP_3-induced $[Ca^{2+}]_m$ increases are established in two steps: (i) IP3R-mediated Ca^{2+} release from ER into cytosol; and (ii) Ca^{2+}-uniporter-mediated membrane potential-dependent Ca^{2+} uptake from cytosol into the mitochondrial matrix.

In order to reproduce the magnitude of IP_3-induced increases of $[Ca^{2+}]_m$ by direct addition of Ca^{2+} to the medium, it was necessary to add 10–15 μM $CaCl_2$ (Figure 3, upper row). Strikingly, these concentrations of $CaCl_2$

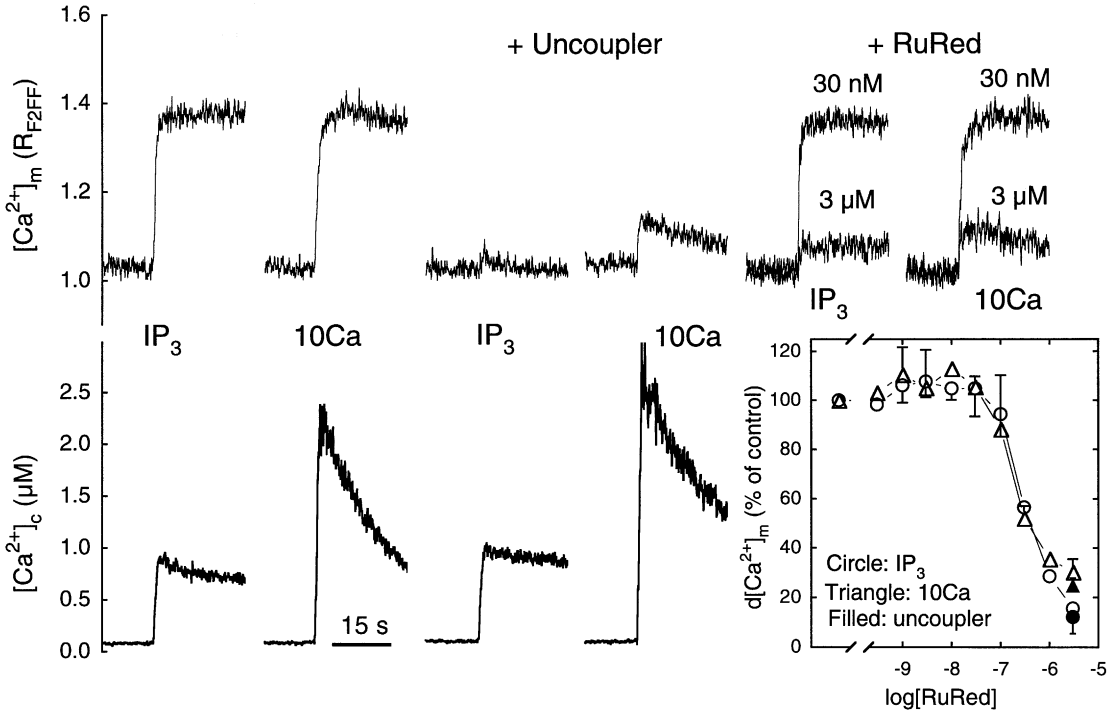

Fig. 3. Simultaneous measurements of $[Ca^{2+}]_c$ and $[Ca^{2+}]_m$ responses evoked by IP_3 and $CaCl_2$ additions in suspensions of fura2FF-loaded permeabilized RBL-2H3 cells. Cytosolic $[Ca^{2+}]$ was followed with rhod2/FA added to the medium (lower panel), and $[Ca^{2+}]_m$ was measured using compartmentalized fura2FF (upper panel). IP_3- (12.5 μM) and $CaCl_2$- (10 μM, '10Ca') induced $[Ca^{2+}]_c$ and $[Ca^{2+}]_m$ responses were recorded in the presence or absence of uncoupler (FCCP/Oligomycin, 5 μg/ml of each, middle panels) or ruthenium red (RuRed, 30 nM or 3 μM, right panel). Inset: dose-dependent inhibition of IP_3- and $CaCl_2$-induced $[Ca^{2+}]_m$ elevation by Ruthenium Red is shown (means ± SE, n = 4–5). The effect of uncoupler (FCCP/Oligomycin, 5 μg/ml of each) measured in the same experiments is shown with filled symbols.

caused much larger increases of $[Ca^{2+}]_c$ than did IP_3 (Figure 3, lower row). These findings show that Ca^{2+} release induced by IP_3 is utilized extremely efficiently to raise $[Ca^{2+}]_m$. This supports the suggestion that IP3Rs may be strategically positioned, allowing mitochondria to sense microdomains of high $[Ca^{2+}]$ generated in the vicinity of activated IP3R (Rizzuto *et al*., 1993, 1994; Hajnóczky *et al*., 1995). Interestingly, Sparagna *et al*. (1995) have described a rapid mode of mitochondrial Ca^{2+} uptake that is activated by relatively small but fast elevations of extramitochondrial $[Ca^{2+}]$ and inhibited by high concentrations of ruthenium red. Since submaximal concentrations of ruthenium red were reported to exert different effects on the standard mode and on the rapid mode of mitochondrial Ca^{2+} uptake (Sparagna *et al*., 1995), we examined the dose response to ruthenium red to test whether the rapid mode was used primarily during uptake of Ca^{2+} released by IP_3. Figure 3 (inset) shows that each concentration of ruthenium red exerted identical effects on $[Ca^{2+}]_m$ responses induced by IP_3 or Ca^{2+} addition, respectively. Since IP_3-induced and Ca^{2+}-induced $[Ca^{2+}]_m$ responses were modulated by ruthenium red in the same manner, it is unlikely that the highly efficient transmission of IP_3-induced Ca^{2+} release into the mitochondria is achieved by utilizing selectively the rapid Ca^{2+} uptake mode.

Another mechanism to underlie the large effect of IP_3 on $[Ca^{2+}]_m$ could be that IP_3 or a metabolite of IP_3 facilitates mitochondrial Ca^{2+} uptake independent of the Ca^{2+} release. This issue was addressed by two experimental approaches. First, $[Ca^{2+}]_m$ increases induced by IP_3 or a slowly metabolized IP_3 analog, 3-deoxy-3-fluoro-IP_3 (FIP_3), or a chemically unrelated activator of IP3R, adenophostin (Takahashi *et al*., 1994), were compared. The same Ca^{2+} release responses and identical rapid increases of $[Ca^{2+}]_m$ were observed in each condition (Figure 4A), suggesting that the metabolism of IP_3 does not play a role in stimulation of mitochondrial Ca^{2+} uptake. Secondly, endoplasic reticulum Ca^{2+} stores were discharged with Tg pretreatment in order to prevent IP_3-induced Ca^{2+} release (Hajnóczky and Thomas 1994, 1997), and, subsequently, the effect of IP_3 on Ca^{2+}-induced mitochondrial Ca^{2+} uptake was studied (Figure 4B). In agreement with previous data obtained with intact cells (Rizzuto *et al*., 1994; Hajnóczky *et al*., 1995), Tg caused a slow and large increase of $[Ca^{2+}]_c$ that was not associated with concurrent elevation of $[Ca^{2+}]_m$. IP_3 did not cause Ca^{2+} release from Tg-pretreated cells and failed to exert any effect on $[Ca^{2+}]_m$ increases induced by subsequent addition of Ca^{2+} (Figure 4B). These observations suggest that an IP_3-dependent conformational change of the uniporter does not account for the large stimulation of mitochondrial Ca^{2+} uptake that is associated with IP_3-induced Ca^{2+} release. Taken together, these data support the idea that IP_3 leads to activation of mitochondrial Ca^{2+} uptake via generation of a localized large increase in $[Ca^{2+}]_c$ in the vicinity of the mitochondria.

Maximal activation of mitochondrial Ca^{2+} uptake during IP_3-induced Ca^{2+} release

In order to estimate the magnitude of the local $[Ca^{2+}]$ increases evoked by IP_3, rates of mitochondrial Ca^{2+}

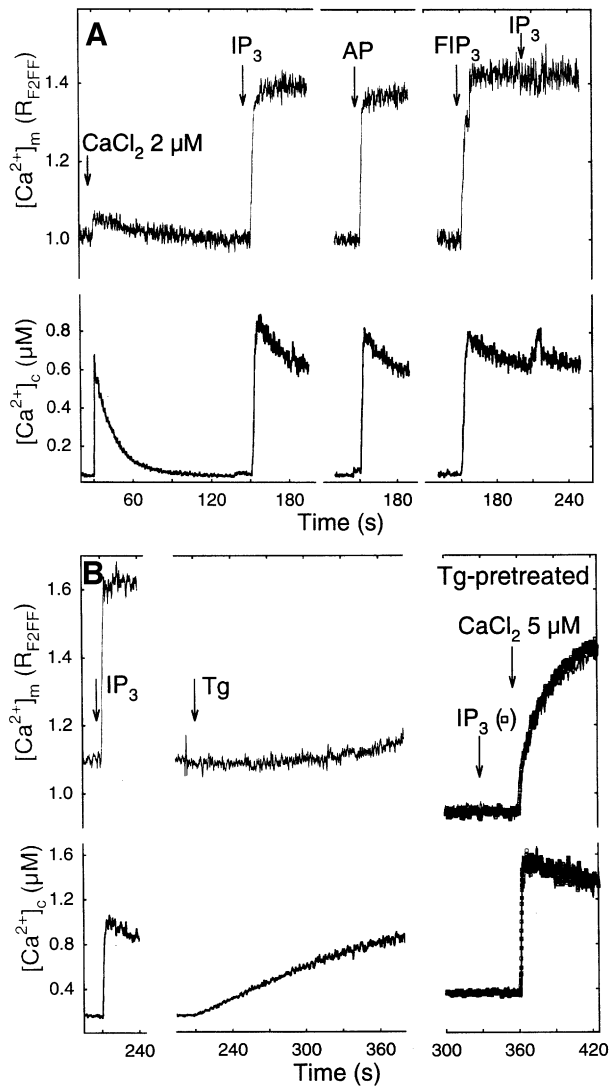

Fig. 4. Effect of IP_3 and IP3R-activation on mitochondrial Ca^{2+} uptake. (**A**) $[Ca^{2+}]_c$ and $[Ca^{2+}]_m$ responses were elicited by different activators of the IP_3R. Supramaximal concentrations of IP_3 (12.5 μM), adenophostin (AP, 2.5 μM) or 3F-IP_3 (FIP_3, 5 μM) were added. In order to optimize Ca^{2+} loading of the ER, $CaCl_2$ (2 μM) was added at the beginning of each run. (**B**) $[Ca^{2+}]_m$ and $[Ca^{2+}]_c$ responses elicited by IP_3 (12.5 μM)-induced Ca^{2+} release (left), by Tg (2 μM)-evoked Ca^{2+} leakage from ER (middle) or by $CaCl_2$ (5 μM) added to Tg-pretreated cells in the presence or absence of IP_3 (right).

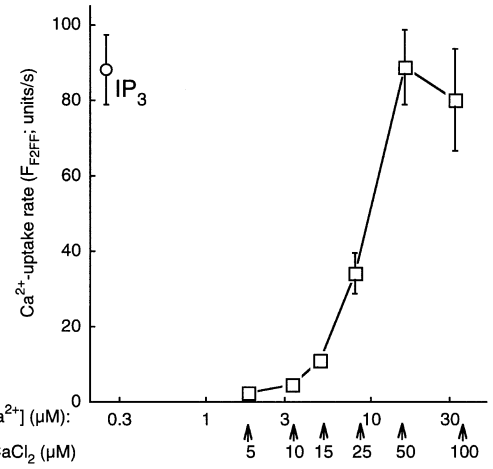

Fig. 5. Maximal activation of mitochondrial Ca^{2+} uptake during IP_3-induced Ca^{2+} release. The rate of mitochondrial Ca^{2+} uptake was measured at varying $[Ca^{2+}]$ obtained by addition of $CaCl_2$ in adherent fura2FF-loaded permeabilized cells. Cytosolic $[Ca^{2+}]$ was calculated using constants obtained from Bers *et al.* (1994). The added $CaCl_2$ concentration values are indicated with arrows below the *x* axis. Data are the average of three separate experiments (mean ± SE).

uptake were measured with varying extramitochondrial $[Ca^{2+}]$, and the rate of Ca^{2+} uptake obtained during IP_3 induced Ca^{2+} release was translated into an effective $[Ca^{2+}]$. This experiment was performed using adherent single cells, since intracellular structures can be preserved better in attached cells than in suspensions of cells during permeabilization (Renard-Rooney *et al.*, 1993; Hajnóczky *et al.*, 1994). The activity of the Ca^{2+} uniporter is manifested in the rate of mitochondrial Ca^{2+} uptake. Figure 5 shows that addition of Ca^{2+} led to dose-dependent increases in mitochondrial Ca^{2+} uptake rates. Half-maximal stimulation was attained at a $[Ca^{2+}]_c$ of ~10 μM, which is in agreement with data obtained using other methods (reviewed in Gunter *et al.*, 1994; Pozzan *et al.*, 1994). Maximal activation was obtained at >16 μM $[Ca^{2+}]_c$, which is similar to the data obtained for permeabilized HeLa cells (Rizzuto *et al.*, 1994) but smaller than the extramitochondrial $[Ca^{2+}]$ required to attain maximal activation of Ca^{2+} uptake by isolated mitochondria. This difference may be due to differences in the allosteric regulation of the uniporter between permeabilized cells and subcellular fractions. It is also noteworthy that measurements of $[Ca^{2+}]_m$ were used to determine the rate of mitochondrial Ca^{2+} uptake in the studies with permeabilized cells, whereas extraluminal $[Ca^{2+}]$ responses were used to calculate Ca^{2+} uptake rates in suspensions of isolated mitochondria.

Remarkably, when IP_3-induced mitochondrial Ca^{2+} uptake was studied under the same conditions in permeabilized cells, the Ca^{2+} uptake rate was as large as it was with maximally effective concentrations of $[Ca^{2+}]$ (Figure 5). Hence, our results show that mitochondrial Ca^{2+} uptake sites were fully activated during Ca^{2+} release induced by maximally effective IP_3. Since maximal rates of mitochondrial Ca^{2+} uptake in response to addition of exogeneous Ca^{2+} were obtained at >16 μM $[Ca^{2+}]_c$, we conclude that the localized increase of $[Ca^{2+}]_c$ caused by IP_3 is >16 μM. Considering that the IP_3-induced global elevations of $[Ca^{2+}]_c$ peak at 400–700 nM in mast cells (Oancea and Meyer, 1996), IP_3-induced Ca^{2+} elevation in the vicinity of the mitochondria can reach values >20-fold higher than the global increases of $[Ca^{2+}]_c$. This appears to involve all mitochondrial uptake sites that participated in uptake of Ca^{2+} during IP_3-induced Ca^{2+} release in permeabilized mast cells.

Although IP_3-linked stimuli exert large effects on $[Ca^{2+}]_m$ and subsequently on mitochondrial metabolism in intact individual cells (Hajnóczky *et al.*, 1995; Rutter *et al.*, 1996), it is not clear whether all or only subsets of mitochondria contribute to the activation of Ca^{2+} accumulation in different cell types. Using mitochondrially targeted aequorin, 30% of the total cellular mitochondrial pool was calculated to be highly responsive to IP_3-linked stimuli in populations of MH75 cells (Rizzuto *et al.*, 1994), whereas in individual CHO cells an essentially

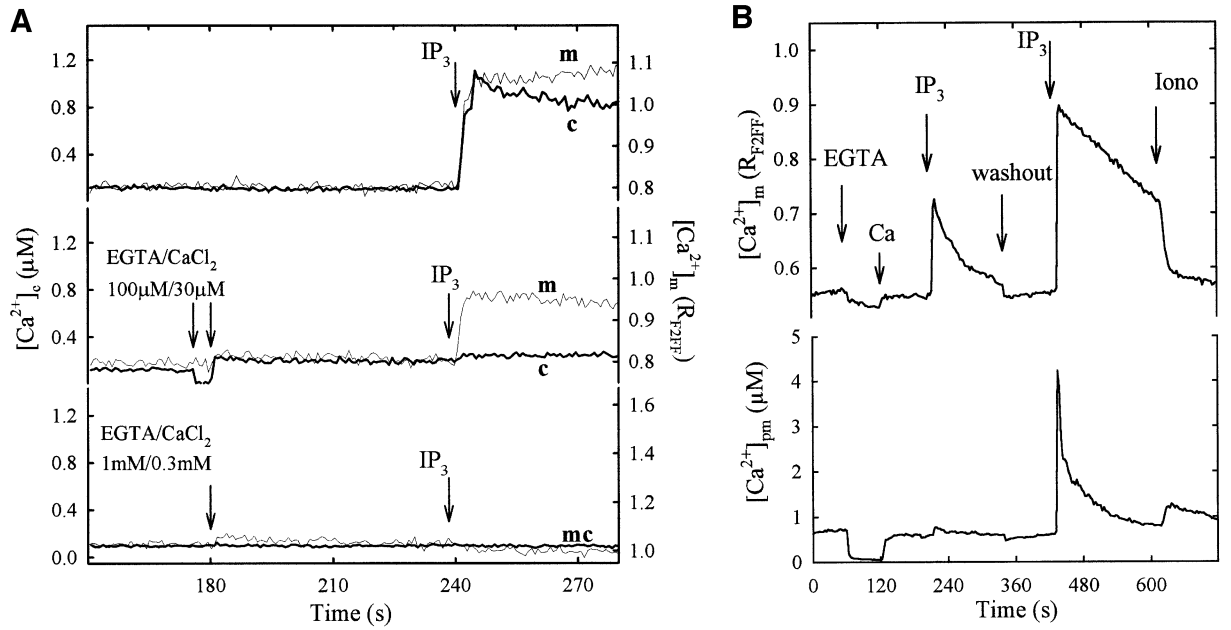

Fig. 6. Effect of Ca^{2+} -EGTA buffer on $[Ca^{2+}]_m$ responses evoked by IP_3. (**A**) Cytosolic $[Ca^{2+}]$ was followed with rhod2/FA added to the medium (hairline) and $[Ca^{2+}]_m$ was measured using compartmentalized fura2FF (thick line) in suspensions of permeabilized RBL-2H3 cells. IP_3- (12.5 μM) induced $[Ca^{2+}]_c$ and $[Ca^{2+}]_m$ responses were recorded in the presence or absence of EGTA titrated with $CaCl_2$ to maintain the preaddition level of $[Ca^{2+}]_c$ (EGTA: 0, upper panel; 100 μM, middle panel; 1 mM, lower panel). (**B**) $[Ca^{2+}]_m$ and $[Ca^{2+}]_{pm}$ responses evoked by IP_3 (12.5 μM) in the presence and absence of Ca^{2+}–EGTA buffer (EGTA 200 μM, $CaCl_2$ 120 μM) were recorded sequentially in an individual fura2FF-loaded permeabilized RBL cell. $[Ca^{2+}]_{pm}$ was monitored using CaGreen-C_{18}. Since CaGreen-C_{18} is associated with all cellular membranes, $[Ca^{2+}]$ in the close vicinity of IP3Rs is detected by only a small fraction of the dye. After the first stimulation with IP_3 (12.5 μM), Ca^{2+} -EGTA and IP_3 were washed out (three changes of medium). In order to facilitate comparison of the $[Ca^{2+}]_m$ responses obtained in the presence and absence of EGTA, a cell with complete reversal of the first $[Ca^{2+}]_m$ response prior to the second addition of IP_3 is shown. In most of the cells, decay of the first $[Ca^{2+}]_m$ response was slower and so the second rise was superimposed on the falling phase of the first elevation.

homogenous increase in $[Ca^{2+}]_m$ was observed across the cells (Rutter *et al*., 1996). Recent studies using aequorin targeted to the intermembrane space indicate that only a small fraction of the mitochondrial inner membrane is exposed to high $[Ca^{2+}]$ microdomains in HeLa cells (Rizzuto *et al*., 1998). Different distributions and densities of IP3Rs in various cells or differences in the spatiotemporal pattern of IP3R activation during stimulation with IP_3-linked stimuli may account for cell-specific mitochondrial responses. Nevertheless, the ability of the IP_3 receptors to evoke maximal activation of all or subsets of mitochondrial Ca^{2+} uptake sites is an extremely significant feature of mitochondrial Ca^{2+} signaling, since the time window for mitochondrial Ca^{2+} uptake is limited during $[Ca^{2+}]_c$ transients evoked by IP_3-linked hormones in intact cells (Hajnóczky *et al*., 1995).

Since IP_3 addition led to saturation of the available mitochondrial Ca^{2+} uptake, these experiments provided information only on the lower limit of IP_3-induced elevations of perimitochondrial $[Ca^{2+}]$. Peak $[Ca^{2+}]_c$ could potentially reach 100 μM or more in the close vicinity of an activated IP3R, as has been calculated for an activated voltage-operated Ca^{2+} channel (reviewed in Neher, 1998). Cytosolic $[Ca^{2+}]$ is estimated to rise to ~100 μM at close proximity to an activated Ca^{2+} channel (<20 nm distance), whereas it peaks at 10–20 μM at 100 nm distance. Slow Ca^{2+} buffers like EGTA are efficient at suppressing global $[Ca^{2+}]_c$ responses and $[Ca^{2+}]_c$ increases at a distance of 100 nm, but fail to attenute the extremely rapid large $[Ca^{2+}]_c$ responses in the 20 nm area. In order to estimate the upper limit of IP_3-induced perimitochondrial $[Ca^{2+}]$

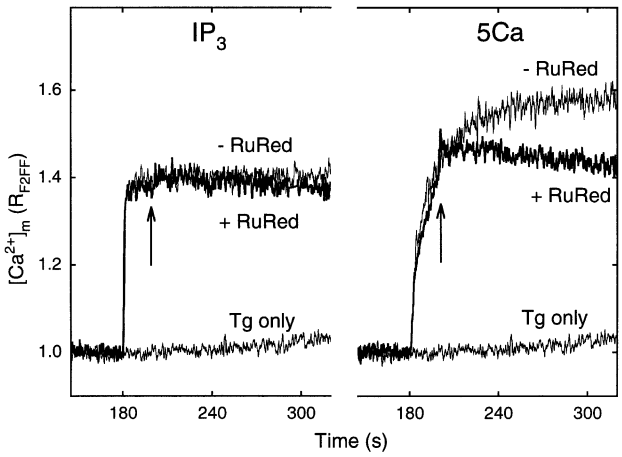

Fig. 7. Transient activation of mitochondrial Ca^{2+} uptake during IP_3-induced Ca^{2+} release. Mitochondrial $[Ca^{2+}]$ responses were recorded in suspensions of fura2FF-loaded permeabilized cells. Ruthenium red (RuRed, 1 μM) was added 20 s after the addition of IP_3 (12.5 μM, left panel) or $CaCl_2$ (5Ca, 5 μM, right panel). In both cases, Ca^{2+} uptake into the ER was blocked by Tg (2 μM) added 5 s before IP_3 or $CaCl_2$.

increases and the average distance between IP3R and mitochondrial Ca^{2+} uptake sites, the effect of EGTA/Ca^{2+} buffer on IP_3-induced $[Ca^{2+}]_c$ and $[Ca^{2+}]_m$ increases was investigated (Figure 6). EGTA was titrated with $CaCl_2$ to maintain the preaddition level of $[Ca^{2+}]_c$, and hence to avoid depletion of Ca^{2+} stores. When EGTA was present at a concentration of 100 μM, the IP_3-induced $[Ca^{2+}]_c$ increase was eliminated (96.5 ± 0.5% inhibition, $n = 4$), but the $[Ca^{2+}]_m$ increase was still observed (58.3 ± 6.3%

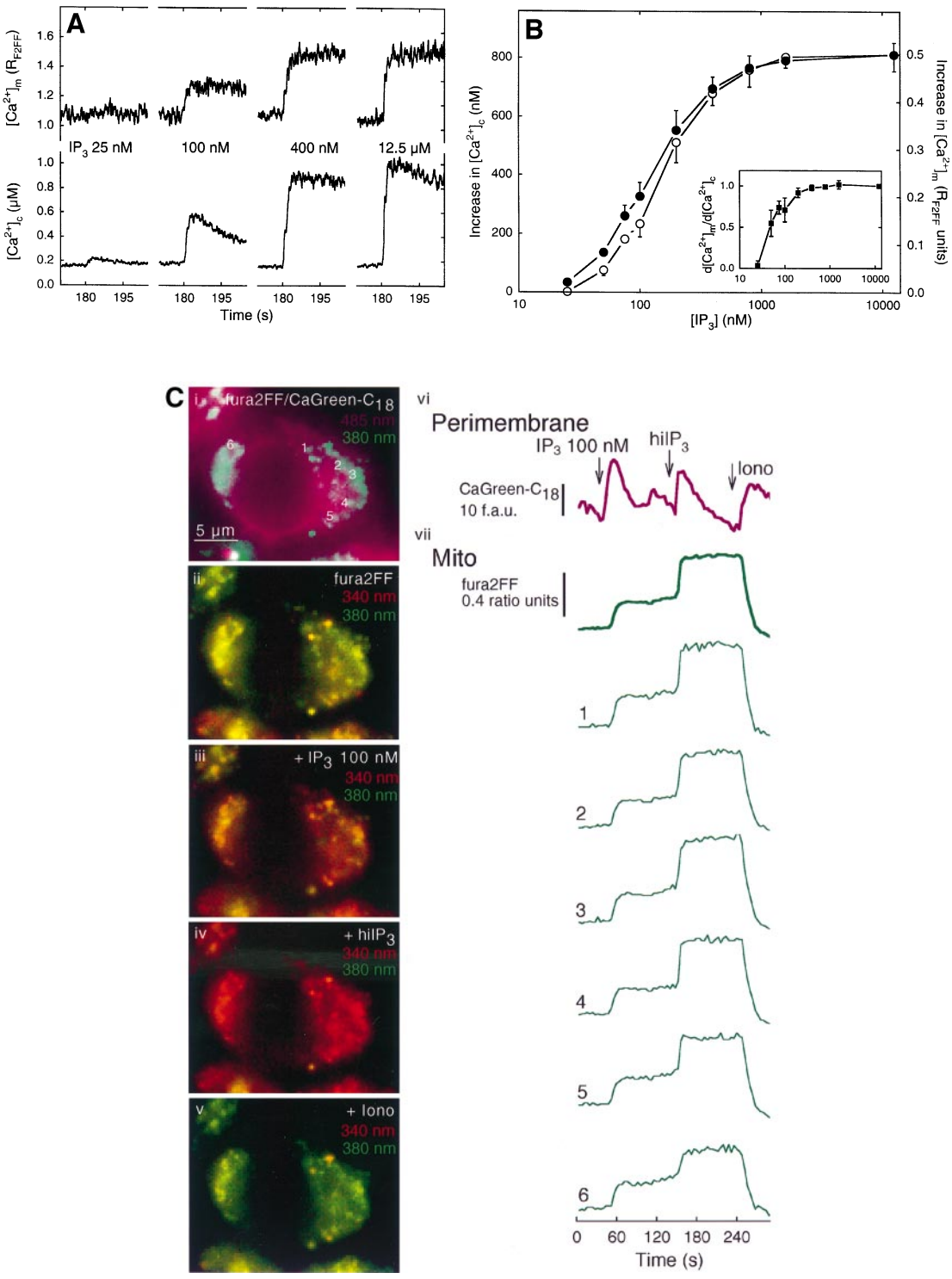

Fig. 8. Quantal properties of IP_3-induced $[Ca^{2+}]_c$ and $[Ca^{2+}]_m$ responses. (**A**) Time courses of $[Ca^{2+}]_c$ and $[Ca^{2+}]_m$ responses elicited by addition of submaximal (25, 100 and 400 nM) and supramaximal (12.5 µM) doses of IP_3 in suspensions of fura2FF-loaded permeabilized cells. (**B**) Dose–response curves of IP_3-induced $[Ca^{2+}]_c$ and $[Ca^{2+}]_m$ responses in suspensions of fura2FF-loaded permeabilized cells are shown with filled and hollow circles, respectively. Data were normalized to the maximum response. Mean ± SE (n = 3–4) are shown. Inset: ratios of the IP_3-induced $[Ca^{2+}]_m$ and $[Ca^{2+}]_c$ responses calculated at each IP_3 concentration are shown. Normalized $[Ca^{2+}]_m$ and $[Ca^{2+}]_c$ responses induced by 25 and 50 nM IP_3 were different at the $P < 0.05$ level. (**C**) $[Ca^{2+}]_m$ and $[Ca^{2+}]_{pm}$ responses evoked by consecutive additions of submaximal (100 nM) and supramaximal (12.5 µM) doses of IP_3 in an individual fura2FF-loaded permeabilized RBL cell are shown. The overlaid images on the left (i–v) show the distribution of the membrane-bound CaGreen-C_{18} (image i, purple) and the mitochondrially compartmentalized fura2FF (image i, green), and the changes in the fura2FF fluorescence (images ii–v, 380 nm green/340 nm red) upon addition of 100 nM IP_3 (ii versus iii), 12.5 µM IP_3 (iii versus iv) and ionomycin (iv versus v). Right: time courses of the global $[Ca^{2+}]_{pm}$ response (vi) and the average $[Ca^{2+}]_m$ response (vii, thick line), and the $[Ca^{2+}]_m$ responses of the marked (1–6 on image i) individual mitochondria (vii, thin lines) are shown.

inhibition, $n = 4$). When EGTA was added in millimolar concentrations (1–10 mM), the IP_3-induced $[Ca^{2+}]_m$ increases were also abolished (100 ± 0% inhibition, $n = 4$). In agreement with the data obtained in permeabilized cell suspensions, the IP_3-induced rise of $[Ca^{2+}]_{pm}$ was essentially abolished, whereas the corresponding $[Ca^{2+}]_m$ response was only partially inhibited by 100–200 μM EGTA in adherent single cells (Figure 6B). Complete inhibition of both responses required 1–10 mM EGTA. It is also shown on Figure 6B that the inhibition exerted by the Ca^{2+} buffer was reversed upon washout of EGTA. These results suggest that the high Ca^{2+} microdomain sensed by the mitochondria is outside of the EGTA-insensitive (100 μM) zone of $[Ca^{2+}]_c$ elevations. Thus, the spatial separation between IP3R and mitochondrial Ca^{2+} uptake sites is probably >10–20 nm and the free Ca^{2+} sensed by the mitochondria is likely to be below 100 μM. By analogy to the voltage-operated Ca^{2+} channel (Neher, 1998), the lower limit of IP_3-induced perimitochondrial $[Ca^{2+}]$ elevations which was calculated to be ~16 μM predicts an average distance of ~100 nm.

Temporal constraints of IP_3-induced mitochondrial Ca^{2+} uptake

IP_3-induced increases of $[Ca^{2+}]_m$ occurred in the form of a rapid rise and a subsequent plateau in the present experiments (Figures 1–4), suggesting that maximal activation of the mitochondrial Ca^{2+} uptake sites lasted at most for a few seconds, despite the sustained rise of $[Ca^{2+}]_c$. It is unlikely that rapid saturation of the mitochondrial fura2FF with Ca^{2+} prevented us from detecting a continuous rise of $[Ca^{2+}]_m$, because omission of the Ca^{2+} prepulse that was applied in most experiments prior to IP_3 addition (shown in Figures 4A and 9) resulted in smaller IP_3-induced Ca^{2+} release and mitochondrial Ca^{2+} uptake responses, with no change in the time-course of $[Ca^{2+}]_m$ (not shown).

Alternatively, a large activation of mitochondrial Ca^{2+} efflux could balance an enhanced mitochondrial Ca^{2+} uptake activity during the plateau phase. In order to determine the activity of the Ca^{2+} uptake component, the effect of ruthenium red added after the rapid upstroke of $[Ca^{2+}]_m$ was studied on IP_3-induced $[Ca^{2+}]_m$ elevations (Figure 7). Since pretreatment with ruthenium red abolished mitochondrial Ca^{2+} accumulations elicited by IP_3 (Figure 3), ruthenium red was expected to cause a fall of $[Ca^{2+}]_m$ if the plateau phase of the IP_3-induced $[Ca^{2+}]_m$ increase was caused by a steady-state between stimulated Ca^{2+} uptake and release. In these experiments, thapsigargin was also added prior to IP_3 so that Ca^{2+} re-uptake into the ER could not attenuate activation of mitochondrial Ca^{2+} accumulation by released Ca^{2+}. Figure 7 shows that only a very slow decrease of the IP_3-dependent $[Ca^{2+}]_m$ response was elicited by ruthenium red applied after the rapid rise of $[Ca^{2+}]_m$, whereas the continuous rise of $[Ca^{2+}]_m$ evoked by addition of exogenous Ca^{2+} was promptly halted by ruthenium red. These results provide evidence that mitochondrial Ca^{2+} uptake falls rapidly following the initial activation during IP_3-induced Ca^{2+} mobilization. The apparent anomaly that sustained $[Ca^{2+}]_c$ increases induced by maximal doses of IP_3-linked hormones were associated with only a single transient increase

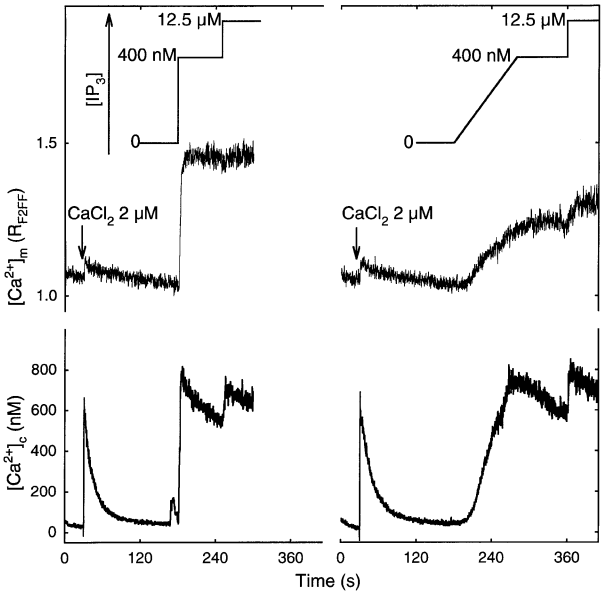

Fig. 9. Control of mitochondrial $[Ca^{2+}]$ uptake by the temporal pattern of IP3R-activation. Time courses of $[Ca^{2+}]_m$ and $[Ca^{2+}]_c$ responses to IP_3 400 nM added as a bolus (left) or gradually over 120 s (right) were measured in suspensions of fura2FF-loaded permeabilized cells. The plots above the traces show the time-course profiles of IP_3 addition. In order to optimize Ca^{2+} loading of the ER, $CaCl_2$ (2 μM) was added at the beginning of each run.

of $[Ca^{2+}]_m$ in intact cells (Hajnóczky *et al.*, 1995) can also be explained by this result.

Quantal calcium responses in the mitochondria

An intriguing and intensively investigated feature of IP_3-induced Ca^{2+} release is the ability of IP_3 dose to control the incremental magnitude of Ca^{2+} release, resulting in the phenomenon of quantal Ca^{2+} mobilization (Muallem *et al.*, 1989; Taylor and Potter, 1990). Figure 8A shows the effects of suboptimal doses of IP_3 on $[Ca^{2+}]_c$ and $[Ca^{2+}]_m$ measured simultaneously in permeabilized cell suspensions. The quantal pattern of IP_3-induced Ca^{2+} release was parallelled by a similar phenomenon of quantal mitochondrial Ca^{2+} uptake (Figure 8A). Importantly, the results shown in Figure 8A represent average responses of cell populations and so the incremental $[Ca^{2+}]_m$ response may reflect cell-to-cell or mitochondrion-to-mitochondrion differences in IP_3 sensitivity, rather than quantal or incremental behavior at the subcellular level. In order to determine whether the incremental $[Ca^{2+}]_m$ response occurs at the level of individual mitochondria, high-spatial-resolution $[Ca^{2+}]_m$ imaging was used to monitor the effect of incremental IP_3 doses. Figure 8C shows global $[Ca^{2+}]_{pm}$ and $[Ca^{2+}]_m$ responses recorded over a single cell, together with the $[Ca^{2+}]_m$ responses of individual mitochondria. Addition of a suboptimal and, subsequently, a maximal dose of IP_3 evoked transient rises of global $[Ca^{2+}]_{pm}$, which were associated with incremental elevations of global $[Ca^{2+}]_m$ (Figure 8C, vi–vii). Although subcellular heterogeneities of the prestimulation fluorescence distribution were observed, elevations of $[Ca^{2+}]_m$ in response to IP_3 increments appeared to be fundamentally homogeneous over the cell, and individual mitochondria largely reflected the incremental Ca^{2+} responses of the whole cell (Figure 8C, ii–vii). In context of the suggestion

Table I. Functional similarities between calcium signal transmission from ER to mitochondria and synaptic transmission

	Calcium signal transmission between ER and mitochondria	Synaptic transmission between cells
Activator	IP3	action potential
Messenger	Ca^{2+}	neurotransmitter
Source	ER through IP3R	synaptic vesicle
Target	Ca^{2+}-uniporter	neurotransmitter receptor
Spatiotemporal organization	Microdomains of high messenger concentration which rapidly dissipate	
	Maximal activation of the targets	
	Quantal pattern of transmission	
	Multiple source units communicate with each target	
	Constitutive/non-vesicular release of the messenger is poorly detected	

that activation of subsets of IP3R with different sensitivities to IP_3 can account for the incremental Ca^{2+} release responses, our data showing the incremental pattern of the corresponding mitochondrial Ca^{2+} uptake suggest that each mitochondrion is functionally linked to multiple subsets of IP3Rs that are activated at each IP_3 concentration.

The connection between IP3Rs and a mitochondrion may be established by two fundamentally different architectures at the level of coupling between individual IP3Rs and mitochondrial Ca^{2+} uptake sites. Mitochondrial Ca^{2+} uptake sites could be activated independently of each other by the Ca^{2+} release through a single IP3R, analogous to the recruitment of Ca^{2+} release through ryanodine receptors by Ca^{2+} entry through single L-type Ca^{2+} channels in the heart (Lopez-Lopez *et al.*, 1995). Alternatively, populations of mitochondrial Ca^{2+} uptake sites could communicate with populations of IP3Rs similarly to the transmission in synapses. Since fluorescence microscopy does not have the resolution to decide whether the Ca^{2+} signal originates from a single channel or from a channel cluster, we designed alternative approaches to this question. If IP3Rs and mitochondrial Ca^{2+} uptake sites are coupled on a one-to-one basis as the first model predicts, cooperation between IP3Rs in activation of mitochondrial Ca^{2+} uptake would not be expected. In contrast, in a quasi-synaptic organization, integration of Ca^{2+} release via multiple IP3Rs at each mitochondrial uptake site could result in cooperative activation. In order to test this possibility, the dose–response curves for IP_3-induced $[Ca^{2+}]_c$ release and for IP_3-induced mitochondrial Ca^{2+} uptake were compared. Cooperation between Ca^{2+} release events supporting mitochondrial Ca^{2+} uptake was expected to appear in a rightward shift and a larger slope of the curve describing the mitochondrial Ca^{2+} response. Figure 8B shows that the curves describing the IP_3 sensitivity of Ca^{2+} release and mitochondrial Ca^{2+} uptake responses are close to each other, but, consistent with the cooperative model, low doses of IP_3 appeared to be less effective at evoking rises of $[Ca^{2+}]_m$ than of $[Ca^{2+}]_c$. This difference is underscored by plotting the ratio of $[Ca^{2+}]_m$ and $[Ca^{2+}]_c$ responses against the concentration of IP_3 (Figure 8B, inset).

It might be argued that we failed to detect $[Ca^{2+}]_m$ responses at the lowest IP_3 concentrations because fura2FF has a low affinity towards Ca^{2+} and so small increases of $[Ca^{2+}]_m$ do not cause measurable fluorescence responses. However, we were also able to show $[Ca^{2+}]_c$ increases at low $[IP_3]$ without a measurable $[Ca^{2+}]_m$ increase, using the higher-affinity rhod2 to measure $[Ca^{2+}]_m$ (not shown). Considering the steep dependence of activation of mitochondrial Ca^{2+} uptake on $[Ca^{2+}]_c$ (Figure 5), it is also possible that increases of IP_3 concentration gradually enhance Ca^{2+} efflux via single IP3Rs and that cooperativity is involved at the level of Ca^{2+} activation of the Ca^{2+} uniporter. This explanation is not likely, however, since by utilizing the positive feedback effect exerted by released Ca^{2+} (reviewed in Berridge, 1993), each IP3R is expected to demonstrate an essentially all-or-none activation during IP_3-induced Ca^{2+} release. Assuming that the concentration of IP_3 controls the number of activated IP3Rs contributing to the Ca^{2+} release, it is most likely that mitochondrial Ca^{2+} uptake is facilitated by cooperation between these Ca^{2+} release sites.

If mitochondrial Ca^{2+} uptake is supported by a positive interaction between IP3R Ca^{2+} release units and the local Ca^{2+} increases generated by IP_3 dissipate rapidly, the temporal pattern of IP3R activation may also play a fundamental role in shaping mitochondrial Ca^{2+} responses. To investigate this issue, bolus addition and gradual infusion of the same dose of IP_3 were applied in suspensions of permeabilized cells, while $[Ca^{2+}]_c$ and $[Ca^{2+}]_m$ were monitored simultaneously (Figure 9). Addition of a 400 nM bolus of IP_3 led to an almost maximal Ca^{2+} release and mitochondrial Ca^{2+} uptake (left traces). When the same dose of IP_3 was injected slowly (the addition was completed in 120 s) the rise of $[Ca^{2+}]_c$ was slow, but the final magnitude was the same as with the bolus addition (right traces). Elevation of $[Ca^{2+}]_m$ was also slow under these conditions, and it is clear that the total response was only 50–60% of the response observed during bolus addition of IP_3 (Figure 9, right traces). This is not a consequence of IP_3 metabolism, since the metabolism-resistant analog of IP_3, FIP_3, also caused smaller $[Ca^{2+}]_m$ responses in continuous infusion than in bolus additions. These results demonstrate that the Ca^{2+} stored in the ER

can be released to a similar extent by either gradual or simultaneous activation of IP3Rs, but simultaneous activation of IP3Rs is required for optimal activation of mitochondrial Ca^{2+} uptake. Taken together, these data show that Ca^{2+} release through multiple IP3Rs is integrated at the level of individual mitochondrial Ca^{2+} uptake sites. This conclusion is also supported by the fact that the average distance between IP3R and mitochondrial Ca^{2+} uptake sites is not in the <20 nm range but may be in the 100 nm range (see above). Microdomains of this size can result from the superposition of the Ca^{2+} contributions of several nearby channels (Dunlap *et al*., 1995; Borst and Sakmann, 1996; Cooper *et al*., 1996).

Remarkably, several features of the IP3R–mitochondrial Ca^{2+} signaling system demonstrated in our study indicate that the functional organization underlying ER–mitochondrial Ca^{2+} coupling is similar to that of synaptic transmission. The corresponding elements of subcellular Ca^{2+} signal transmission and synaptic transmission and their common functional features are listed in Table I. The molecular microstructure underlying Ca^{2+} signal transmission between ER and mitochondria has not been explored, but the close apposition of ER and mitochondrial membranes is well known and there are reports demonstrating clusters of IP3Rs in ER membranes facing mitochondria (Shore and Tata, 1977; Maeda *et al*., 1989; Mignery *et al*., 1989; Satoh *et al*., 1990; Rizzuto *et al*., 1998). Assuming that the matching regions of the mitochondria are rich in Ca^{2+} uniporters, these areas may provide the surface for Ca^{2+} signal transmission from IP3Rs to mitochondrial Ca^{2+} uptake sites. Release of Ca^{2+} from the ER occurs in a quantal manner in response to IP_3, similar to neurotransmitter release in response to Ca^{2+} entry through voltage-operated Ca^{2+} channels (del Castillo and Katz, 1954; Katz, 1969). Microdomains of high $[Ca^{2+}]$ with a short lifetime are built up at the ER-mitochondrial junctions, analogous to the large transients of neurotransmitter concentration in the synaptic cleft. Diffusion and re-uptake of the messenger are involved in the rapid clearance in both cases. Several lines of evidences suggest that each mitochondrial Ca^{2+} uptake site is supported by Ca^{2+} release occurring through more than one IP3R, which is compatible with the fact that each postsynaptic receptor can be activated by neurotransmitter release from more than one synaptic vesicle. This coupling pattern is different from the Ca^{2+} coupling between the dihydropyridine Ca^{2+} channel and the ryanodine receptor, where single Ca^{2+} channels activate ryanodine receptors independently of one other. Furthermore, the IP3R–mitochondrial Ca^{2+} uptake site coupling shows maximal efficiency in activation of the Ca^{2+} uniporter, just as maximal activation of the neurotransmitter receptors can be obtained during neurotransmitter release in the synapses. Our study shows that synchronized activation of IP3Rs is required for optimal activation of mitochondrial Ca^{2+} uptake sites, whereas saturation of postsynaptic receptors may require a single quantum of neurotransmitter or more (reviewed in Frerking and Wilson, 1996). Constitutive release of the messenger at the ER–mitochondrial junction triggered by thapsigargin is poorly detected by the mitochondrial Ca^{2+} uptake sites, just as non-vesicular release of the neurotransmitter is detected with low efficiency at the synapses. Taken together, our data show that Ca^{2+} signal transmission between intracellular organelles can utilize a closely related functional architecture to that used for synaptic signal propagation between cells.

Conclusions

This work describes fundamental features of the local Ca^{2+} regulation that supports communication between endoplasmic reticulum and mitochondria. We show that Ca^{2+} release through IP3Rs leads to maximal but short-lasting activation of mitochondrial Ca^{2+} uptake and that this response is explained by the generation of large perimitochondrial $[Ca^{2+}]$ spikes. Localized increases of $[Ca^{2+}]_c$ peak over 15 μM and these responses are at least 20-fold larger than the global $[Ca^{2+}]_c$ elevations. Furthermore, we show that quantal Ca^{2+} release via IP3Rs yields quantal mitochondrial Ca^{2+} uptake, even at the level of individual mitochondria. Although this suggests that single IP3Rs are effective at raising $[Ca^{2+}]_m$, optimal activation of mitochondrial Ca^{2+} uptake is obtained by synchronous activation of IP3Rs. Thus, the IP3R-mediated elementary Ca^{2+} release signals which represent the building blocks of cytosolic Ca^{2+} signaling may stimulate mitochondrial Ca^{2+} uptake on an individual basis, but recruitment of multiple elementary events leads to disproportionally larger mitochondrial $[Ca^{2+}]$ responses. Since calcium signaling involves temporal and spatial coordination of the elementary Ca^{2+} release events, calcium spikes and oscillations evoked by synchronized and periodic activation of IP3Rs become particularly effective in establishing dynamic control over mitochondrial $[Ca^{2+}]$, and in turn, cellular energy metabolism.

Materials and methods

Cells

RBL-2H3 mucosal mast cells (kindly provided by Clare Fewtrell) were cultured in Eagle's minimum essential medium supplemented with 20% (v/v) fetal bovine serum, 4 mM glutamine, 100 U/ml penicillin and 100 μg/ml streptomycin in 5% CO_2 and 95% air at 37°C (Taurog *et al*., 1979). For imaging measurements, cells were plated onto poly-D-lysine-coated coverslips and cultured for 4–5 days prior to experiments. For cell suspension studies, cells were cultured for 6 days in 75 cm^2 flasks.

Transfection of cells for fluorescence imaging

Cells plated onto poly-D-lysine-coated coverslips were transfected with plasmid DNA (1 μg/ml of pCMV/*myc*/mito/GFP for 7 h, Invitrogen) using Lipofectamine (10 μg/ml) and OPTI-MEM medium (Life Technologies). Cells were observed 24 h after transfection.

Fluorescence imaging measurements in permeabilized RBL-2H3 cells

Prior to use, the cells were preincubated for 30 min in extracellular medium (ECM) composed of 121 mM NaCl, 5 mM $NaHCO_3$, 10 mM Na–HEPES, 4.7 mM KCl, 1.2 mM KH_2PO_4, 1.2 mM $MgSO_4$, 2 mM $CaCl_2$, 10 mM glucose and 2% bovine serum albumin (BSA) pH 7.4 at 37°C. For measurements of $[Ca^{2+}]_m$, the cells were loaded with 5 μM fura2FF/AM or 2 μM rhod2/AM in the presence of 0.003% (w/v) pluronic acid for 50–70 min. In order to label mitochondria, the cells were loaded with the vital dye MitoTracker Red (50 nM) for 30–45 min. Dye-loaded cells were washed with Ca^{2+}-free extracellular buffer composed of 120 mM NaCl, 20 mM Na–HEPES, 5 mM KCl, 1 mM KH_2PO_4, 100 μM EGTA/Tris pH 7.4 and then permeabilized by incubation for 5 min with 15 μg/ml digitonin in intracellular medium (ICM) composed of 120 mM KCl, 10 mM NaCl, 1 mM KH_2PO_4, 20 mM Tris–HEPES pH 7.2 with 2 mM MgATP, 2 mM succinate and 1 μg/ml each of antipain, leupeptin and pepstatin. ICM was passed through a Chelex column prior to addition of ATP and protease inhibitors to lower the ambient $[Ca^{2+}]$. The medium free $[Ca^{2+}]$ was <100 nM

after Chelex treatment and did not exceed 300–400 nM after addition of ATP, succinate and protease inhibitors. In most of the experiments, 20 μM EGTA/Tris was also present during permeabilization in order to decrease $[Ca^{2+}]$ (<50 nM). For measurements of $[Ca^{2+}]_{pm}$, labeling of cells with CaGreen-C18 or fura-C18 (1.5–5 μM) was carried out during permeabilization. After permeabilization, the cells were washed into fresh buffer without digitonin and incubated in the imaging chamber, at 35°C.

Fluorescence images were acquired using an Olympus IX70 inverted microscope fitted with either 40× (UApo, NA 0.65–1.35) or 100× (UPlanApo, NA 0.5–1.35) oil immersion objective and a cooled CCD camera (PXL, Photometrics) under computer control. The computer also controlled a filter wheel or a scanning monochromator (DeltaRam, PTI) to select the excitation wavelength. Excitation at 340 and 380 nm was used for fura2FF and for fura-C18, respectively; 380 nm was used for mitoGFP, 490 nm for CaGreen-C18, 545 nm for rhod2 and 570 nm for MitoTracker Red, with multiwavelength beamsplitter/emission filter combinations that allowed simultaneous measurement of fura2FF and CaGreen-C18 fluorescence, or fura-C18 and rhod2 fluorescence, or mitoGFP and MitoTracker Red fluorescence, or mitoGFP and rhod2 fluorescence, or fura2FF, CaGreen-C18 and MitoTracker Red fluorescence (Chroma Technology Corp.). $[Ca^{2+}]_m$ in fura2FF-loaded individual permeabilized cells was calculated from the fluorescence ratio derived from image pairs obtained with 340 and 380 nm excitation using a K_d for Ca^{2+} of 35 μM (A.Minta, Teflabs).

Experiments were carried out with at least four different cell preparations, and 20–60 cells were monitored in each experiment. Traces represent single-cell or single-mitochondrion responses unless indicated otherwise.

Fluorometric measurements of $[Ca^{2+}]_c$ and $[Ca^{2+}]_m$ in suspensions of permeabilized RBL-2H3 cells

Measurements of $[Ca^{2+}]_m$ were carried out by first loading the intact cells for 60 min with 5 μM Fura2FF/AM in ECM supplemented with 0.003% of pluronic acid at 37°C. Fura2FF-loaded cells were detached using Trypsin-Versene (BioWhittaker), washed in Ca^{2+}-free extracellular buffer (125 g for 4 min) and stored on ice. The cells (~2.4 mg protein/1.8 ml) were permeabilized using 25 μg/ml digitonin for 6 min in ICM at 35°C, followed by washout of the released cytosolic fura2FF (125 *g* for 4 min). Permeabilized cells were resuspended in ICM supplemented with 0.25 μM rhod2/FA and maintained in a stirred thermostated cuvette at 35°C. In most experiments, 2 μM $CaCl_2$ was added after permeabilization (shown in Figures 3A and 8) to facilitate loading of the ER Ca^{2+} store. Fluorescence was monitored in a multiwavelength-excitation dual-wavelength-emission fluorimeter (DeltaRAM, PTI) using 340 and 380 nm excitation, and 500 nm emission for fura2FF, and 540 nm excitation and 580 nm emission for rhod2.

Calibration of the rhod2 signal was carried out at the end of each measurement, adding 1.5 mM $CaCl_2$, and subsequently EGTA/Tris 10 mM pH 8.5. $[Ca^{2+}]_c$ was calculated by using a K_d of 1 μM (A.Minta, Teflabs).

Calcium release induced by IP_3 was found to be utilized extremely efficiently to raise $[Ca^{2+}]_m$ in suspensions of permeabilized cells, though even stronger coupling between Ca^{2+} release and mitochondrial Ca^{2+} uptake was observed in adherent permeabilized cells (mitochondrial Ca^{2+} uptake rates are translated into an effective perimitochondrial $[Ca^{2+}]$ of 3–5 μM and >16 μM, respectively). This difference is probably to due to a better preservation of intracellular structures, particularly the connections between ER and mitochondria in adherent permeabilized cells (Renard-Rooney *et al*., 1993; Hajnóczky *et al*., 1994). Hence, the technically less-difficult suspension experiments were used for pharmacological tests, whereas imaging of adherent permeabilized cells was used to estimate the maximal efficiency of Ca^{2+} signal transmission between ER and mitochondria and to visualize $[Ca^{2+}]_m$ signals at subcellular resolution.

Experiments were carried out with 3–4 different cell preparations.

Acknowledgements

We would like to thank Drs Tamás Balla, Sandor Györke, Jan Hoek and Bob Silver for helpful discussions. We are greatly indebted to Drs Clare Fewtrell and M.Takahashi for providing us with RBL-2H3 cells and adenophostin, respectively. This work was supported by National Institutes of Health grant DK51526 and by the Burroughs Wellcome Fund Career Award in the Biomedical Sciences #272 to G.H.

References

Babcock,D.F., Herrington,J., Goodwin,P.C., Park,Y.B. and Hille,B. (1997) Mitochondrial participation in the intracellular Ca^{2+} network. *J. Cell. Biol.*, **136**, 833–844.

Berridge,M.J. (1993) Inositol trisphosphate and calcium signalling. *Nature*, **361**, 315–325.

Berridge,M.J. (1997) The AM and FM of calcium signalling. *Nature*, **386**, 759–760.

Bers,D.M., Patton,C.W. and Nuccitelli,R. (1994) A practical guide to the preparation of Ca^{2+} buffers. *Methods Cell Biol.*, **40**, 3–29.

Bootman,M.D. and Berridge,M.J. (1996) Subcellular Ca^{2+} signals underlying waves and graded responses in HeLa cells. *Curr. Biol.*, **6**, 855–865.

Bootman,M.D., Berridge,M.J. and Lipp,P. (1997) Cooking with calcium: the recipes for composing global signals from elementary events. *Cell*, **91**, 367–373.

Borst,J.G. and Sakmann,B. (1996) Calcium influx and transmitter release in a fast CNS synapse. *Nature*, **383**, 431–434.

Budd,S.L. and Nicholls,D.G. (1996) Mitochondria, calcium regulation and acute glutamate excitotoxicity in cultured cerebellar granule cells. *J. Neurochem.*, **67**, 2282–2291.

Clapham,D.E. (1995) Calcium signaling. *Cell*, **80**, 259–268.

Cobbold,P.H. and Cuthbertson,K.S. (1990) Calcium oscillations: phenomena, mechanisms and significance. *Semin. Cell Biol.*, **1**, 311–321.

Cooper,R.L., Winslow,J.L., Govind,C.K. and Atwood,H.L. (1996) Synaptic structural complexity as a factor enhancing probability of calcium-mediated transmitter release. *J. Neurophysiol.*, **75**, 2451–2466.

De Koninck,P. and Schulman,H. (1998) Sensitivity of CaM kinase II to the frequency of Ca^{2+} oscillations. *Science*, **279**, 227–230.

del Castillo,J. and Katz,B. (1954) Quantal components of the endplate potential. *J. Physiol.*, **124**, 560–573.

Dolmetsch,R.E., Lewis,R.S., Goodnow,C.C. and Healy,J.I. (1997) Differential activation of transcription factors induced by Ca^{2+} response amplitude and duration. *Nature*, **386**, 855–858.

Dunlap,K., Luebke,J.I. and Turner,T.J. (1995) Exocytotic Ca^{2+} channels in mammalian central neurons. *Trends Neurosci.*, **18**, 89–98.

Frerking,M. and Wilson,M. (1996) Saturation of postsynaptic receptors at central synapses? *Curr. Opin. Neurobiol.*, **6**, 395–403.

Golovina,V.A. and Blaustein,M.P. (1997) Spatially and functionally distinct Ca^{2+} stores in sarcoplasmic and endoplasmic reticulum. *Science*, **275**, 1643–1648.

Gunter,T.E., Gunter,K.K., Sheu,S.S. and Gavin,C.E. (1994) Mitochondrial calcium transport: physiological and pathological relevance. *Am. J. Physiol.*, **267**, C313–C339.

Hajnóczky,G. and Thomas,A.P. (1994) The inositol trisphosphate calcium channel is inactivated by inositol trisphosphate. *Nature*, **370**, 474–477.

Hajnóczky,G. and Thomas,A.P. (1997) Minimal requirements for calcium oscillations driven by the IP_3 receptor. *EMBO J.*, **16**, 3533–3543.

Hajnóczky,G., Lin,C. and Thomas,A.P. (1994) Luminal communication between intracellular calcium stores modulated by GTP and the cytoskeleton. *J. Biol. Chem.*, **269**, 10280–10287.

Hajnóczky,G., Robb-Gaspers,L.D., Seitz,M.B. and Thomas,A.P. (1995) Decoding of cytosolic calcium oscillations in the mitochondria. *Cell*, **82**, 415–424.

Hanson,P.I., Meyer,T., Stryer,L. and Schulman,H. (1994) Dual role of calmodulin in autophosphorylation of multifunctional CaM kinase may underlie decoding of calcium signals. *Neuron*, **12**, 943–956.

Horne,J.H. and Meyer,T. (1997) Elementary calcium-release units induced by inositol trisphosphate. *Science*, **276**, 1690–1693.

Hoth,M., Fanger,C.M. and Lewis,R.S. (1997) Mitochondrial regulation of store-operated calcium signaling in T lymphocytes. *J. Cell. Biol.*, **137**, 633–648.

Houslay,M.D. and Milligan,G. (1997) Tailoring cAMP-signalling responses through isoform multiplicity. *Trends Biochem. Sci.*, **22**, 217–224.

Ichas,F., Jouaville,L.S. and Mazat,J.P. (1997) Mitochondria are excitable organelles capable of generating and conveying electrical and calcium signals. *Cell*, **89**, 1145–1153.

Jouaville,L.S., Ichas,F., Holmuhamedov,E.L., Camacho,P. and Lechleiter,J.D. (1995) Synchronization of calcium waves by mitochondrial substrates in *Xenopus laevis* oocytes. *Nature*, **377**, 438–441.

Katz,B. (1969) *The Release of Neural Transmitter Substances*. Liverpool University Press, Liverpool, UK.

Kim,T.D., Eddlestone,G.T., Mahmoud,S.F., Kuchtey,J. and Fewtrell,C. (1997) Correlating Ca^{2+} responses and secretion in individual RBL-2H3 mucosal mast cells. *J. Biol. Chem.*, **272**, 31225–31229.

Lester,L.B. and Scott,J.D. (1997) Anchoring and scaffold proteins for kinases and phosphatases. *Recent Prog. Horm. Res.*, **52**, 409–429.

Llinas,R., Sugimori,M. and Silver,R.B. (1992) Microdomains of high calcium concentration in a presynaptic terminal. *Science*, **256**, 677–679.

Lopez-Lopez,J.R., Shacklock,P.S., Balke,C.W. and Wier,W.G. (1995) Local calcium transients triggered by single L-type calcium channel currents in cardiac cells. *Science*, **268**, 1042–1045.

Maeda,N., Niinobe,M., Inoue,Y. and Mikoshiba,K. (1989) Developmental expression and intracellular location of P400 protein characteristic of Purkinje cells in the mouse cerebellum. *Dev. Biol.*, **133**, 67–76.

Marsault,R., Murgia,M., Pozzan,T. and Rizzuto,R. (1997) Domains of high Ca^{2+} beneath the plasma membrane of living A7r5 cells. *EMBO J.*, **16**, 1575–1581.

McCormack,J.G., Halestrap,A.P. and Denton,R.M. (1990) Role of calcium ions in regulation of mammalian intramitochondrial metabolism. *Physiol. Rev.*, **70**, 391–425.

Mignery,G.A., Sudhof,T.C., Takei,K. and De Camilli,P. (1989) Putative receptor for inositol 1,4,5-trisphosphate similar to ryanodine receptor. *Nature*, **342**, 192–195.

Muallem,S., Pandol,S.J. and Beeker,T.G. (1989) Hormone-evoked calcium release from intracellular stores is a quantal process. *J. Biol. Chem.*, **264**, 205–212.

Neher,E. (1998) Vesicle pools and Ca^{2+} microdomains: new tools for understanding their roles in neurotransmitter release. *Neuron*, **20**, 389–399.

Oancea,E. and Meyer,T. (1996) Reversible desensitization of inositol trisphosphate-induced calcium release provides a mechanism for repetitive calcium spikes. *J. Biol. Chem.*, **271**, 17253–17260.

Parker,I. and Yao,Y. (1996) Ca^{2+} transients associated with openings of inositol trisphosphate-gated channels in Xenopus oocytes. *J. Physiol. (Lond.)*, **491**, 663–668.

Parker,I., Choi,J. and Yao,Y. (1996) Elementary events of InsP3-induced Ca^{2+} liberation in *Xenopus* oocytes: hot spots, puffs and blips. *Cell Calcium*, **20**, 105–121.

Pawson,T. and Scott,J.D. (1997) Signaling through scaffold, anchoring and adaptor proteins. *Science*, **278**, 2075–2080.

Petersen,O.H., Petersen,C.C. and Kasai,H. (1994) Calcium and hormone action. *Annu. Rev. Physiol.*, **56**, 297–319.

Pozzan,T., Rizzuto,R., Volpe,P. and Meldolesi,J. (1994) Molecular and cellular physiology of intracellular calcium stores. *Physiol. Rev.*, **74**, 595–636.

Pralong,W.F., Spät,A. and Wollheim,C.B. (1994) Dynamic pacing of cell metabolism by intracellular Ca^{2+} transients. *J. Biol. Chem.*, **269**, 27310–27314.

Putney,J.W.,Jr (1998) Calcium Signaling: Up, Down, Up, Down. What's the Point? *Science*, **279**, 191–192.

Reber,B.F.X. and Schindelholz,B. (1996) Detection of a trigger zone of bradykinin-induced fast calcium waves in PC12 neurites. *Pflugers Arch.*, **432**, 893–903.

Renard-Rooney,D.C., Hajnóczky,G., Seitz,M.B., Schneider,T.G. and Thomas,A.P. (1993) Imaging of inositol 1,4,5-trisphosphate-induced Ca^{2+} fluxes in single permeabilized hepatocytes. Demonstration of both quantal and nonquantal patterns of Ca^{2+} release. *J. Biol. Chem.*, **268**, 23601–23610.

Rizzuto,R., Simpson,A.W., Brini,M. and Pozzan,T. (1992) Rapid changes of mitochondrial Ca^{2+} revealed by specifically targeted recombinantaequorin. *Nature*, **358**, 325–327.

Rizzuto,R., Brini,M., Murgia,M. and Pozzan,T. (1993) Microdomains with high Ca^{2+} close to IP_3-sensitive channels that are sensed by neighboring mitochondria. *Science*, **262**, 744–747.

Rizzuto,R., Bastianutto,C., Brini,M., Murgia,M. and Pozzan,T. (1994) Mitochondrial Ca^{2+} homeostasis in intact cells. *J. Cell. Biol.*, **126**, 1183–1194.

Rizzuto,R., Pinton,P., Carrington,W., Fay,F.S., Fogarty,K.E., Lifshitz,L.M., Tuft,R.A. and Pozzan,T. (1998) Close contacts with the endoplasmic reticulum as determinants of mitochondrial Ca^{2+} responses. *Science*, **280**, 1763–1766.

Rutter,G.A., Burnett,P., Rizzuto,R., Brini,M., Murgia,M., Pozzan,T., Tavare,J.M and Denton,R.M. (1996) Subcellular imaging of intramitochondrial Ca^{2+} with recombinant targeted aequorin: significance for the regulation of pyruvate dehydrogenase activity. *Proc. Natl Acad. Sci. USA*, **93**, 5489–5494.

Satoh,T., Ross,C.A., Villa,A., Supattapone,S., Pozzan,T., Snyder,S.H. and Meldolesi,J. (1990) The inositol 1,4,5-trisphosphate receptor in cerebellar Purkinje cells: quantitative immunogold labeling reveals concentration in an ER subcompartment. *J. Cell. Biol.*, **111**, 615–624.

Shore,G.C. and Tata,J.R. (1977) Two fractions of rough endoplasmic reticulum from rat liver. *J. Cell. Biol.*, **72**, 714–725.

Silver,R.A., Lamb,A.G. and Bolsover,S.R. (1990) Calcium hotspots caused by L-channel clustering promote morphological changes in neuronal growth cones. *Nature*, **343**, 751–754.

Simpson,P.B., Mehotra,S., Lange,G.D. and Russell,J.T. (1997) High density distribution of endoplasmic reticulum proteins and mitochondria at specialized Ca^{2+} release sites in oligodendrocyte processes. *J. Biol. Chem.*, **272**, 22654–22661.

Sparagna,G.C., Gunter,K.K., Sheu,S.S. and Gunter,T.E. (1995) Mitochondrial calcium uptake from physiological-type pulses of calcium. A description of the rapid uptake mode. *J. Biol. Chem.*, **270**, 27510–27515.

Takahashi,M., Tanzawa,K. and Takahashi,S. (1994) Adenophostins, newly discovered metabolites of Penicillium brevicompactum, act as potent agonists of the inositol 1,4,5-trisphosphate receptor. *J. Biol. Chem.*, **269**, 369–372.

Tanimura,A. and Turner,R.J. (1996) Inositol 1,4,5-trisphosphate-dependent oscillations of luminal $[Ca^{2+}]$ in permeabilized HSY cells. *J. Biol. Chem.*, **271**, 30904–30908.

Taurog,J.D., Fewtrell,C. and Becker,E.L. (1979) IgE mediated triggering of rat basophil leukemia cells: lack of evidence for serine esterase activation. *J. Immunol.*, **122**, 2150–2153.

Taylor,C.W. and Potter,B.V.L. (1990) The size of inositol 1,4,5-trisphosphate-sensitive Ca^{2+} stores depends on inositol 1,4,5-trisphosphate concentration. *Biochem. J.*, **266**, 189–194.

Thomas,A.P., Bird,G.S., Hajnóczky,G., Robb-Gaspers,L.D. and Putney,J.W.,Jr (1996) Spatial and temporal aspects of cellular calcium signaling. *FASEB J.*, **10**, 1505–1517.

Tse,A., Tse,F.W., Almers,W. and Hille,B. (1993) Rhythmic exocytosis stimulated by GnRH-induced calcium oscillations in rat gonadotropes. *Science*, **260**, 82–84.

Yao,Y., Choi,J. and Parker,I. (1995) Quantal puffs of intracellular Ca^{2+} evoked by inositol trisphosphate in *Xenopus* oocytes. *J. Physiol. (Lond)*, **482**, 533–553.

Received August 10, 1998; revised November 4, 1998; accepted November 5, 1998